Al-Khwarizmi Engineering Journal, Vol. 10, No. 2, P.P. 32- 48 (2014)

Al-Khwarizmi Engineering Journal

Comparisons of Mechanical Properties of sub-mm Lead Based and Lead Free Based Solder Using in Manufacturing of Printed Circuits

Alaa Hasan Ali

Department of Materials Engineering/University of Technology

Sabbatical leave in Chemical Engineering& Materials Science Department/ Michigan State University/ USA

Email: dr_alaahassan@yahoo.com

(Received 22 February 2013; accepted 18 June 2014)

Abstract

This study investigates the mechanical compression properties of tin-lead and lead-free alloy spherical balls, using more than 500 samples to identify statistical variability in the properties in each alloy. Isothermal aging was done to study and compare the aging effect on the microstructure and properties.

The results showed significant elastic and plastic anisotropy of tin phase in lead-free tin based solder and that was compared with simulation using a Crystal Plasticity Finite Element (CPEF) method that has the anisotropy of Sn installed. The results and experiments were in good agreement, indicating the range of values expected with anisotropic properties.

Keywords: *Lead-free solder, composite solder, and aging.*

1. Introduction

Lead based solders have been widely used in electronic assembly industry for several decades. However due to potential hazards associated with the toxicity of lead affords has been taken to eliminate or replace the tin in consumer products. Among these efforts, tin based solders have become the dominant choice for electronic assembly industries.

In recent years, there have been many investigations regarding the mechanical properties of the lead-free solders [1, 2]. However there is lack of understanding about the mechanical properties of these alloys. The existing information in the literature are from a different fabrication and testing process which causes variation in microstructures and mechanical properties associated with these microstructures [3]. Therefore in order to develop a reliable model to predict the deformation behavior of lead-free solders, a comprehensive understanding of mechanical properties is required.

Most of the prior studies focus on the tin anisotropy and the effect of this material characteristic on mechanical properties of lead-free solder joints and their behavior during mechanical deformation and thermal processes [4, 5, 6]. There are very few investigations on the statistical variation of mechanical properties of as fabricated lead-free solder balls [1, 7]. Therefore Further investigations are required to be conducted to provide more insights into the effects of processing parameters and also alloy compositions on the mechanical properties of different solders. The focus of this study is to provide enough statistical data to be able to compare the joint scale mechanical behavior of the lead free solders and different lead based solders to gain insights into the effect of anisotropy associated with the coarse grain microstructure of lead free solders with isotropic properties of lead based solders.

Due to the isotropy associated with the polycrystalline microstructure of lead based solder as well as the interaction between different phases (Pb as a soft phase and tin as a hard phase) traditional modeling procedures based upon the isotropic hardening and creep models can be quite efficient in prediction of damage in electronic packages specially in the thermal cycling loading conditions [6, 8, 9]. However use of these methods for prediction of the location of failure is not promising in lead free solders.

Previous work focus on the variability of solder balls of different alloys and their effect on manufacturing electronic system. Additional work ought to be done to improve the scientific understanding variable properties of solder balls for different alloys so the motives of the present study are to give more understanding how the different balls sizes and Sn elastic and Plastic anisotropy phenomena effect on the strength and ratability of solder joint of manufactured electron system and must be taken into consideration by manufacturer and supplier.

2. Crystal Plasticity Formulation

A velocity gradient in plastic deformation in the material coordinate system can be decomposed into a rate of deformation and a spin tensor as:

$$L^P = D^P + W^P \qquad \ldots(1)$$

Where L^P is the velocity gradient in plastic deformation. D^P and W^P are rate of deformation and spin tensor simultaneously.

An elasto-plastic problem is usually defined as a constrained optimization problem aimed at finding the optimum stress tensor and internal variables for a given strain increment. In such a problem, the objective function is defined based on the principle of maximum dissipation and is made of terms describing the incremental release of elastic strain energy and the dissipation due to the incremental plastic work and the constraint is the yield function, [10].

$$(\sigma_{j+1}, q_{j+1}) = \begin{cases} \text{Min}\left[I(x) = \left(\sigma_{j+1}^{trial} - \sum\right) : C^{-1} : \left(\sigma_{j+1}^{trial} - \sum\right) + (q - q_j) : E^{-1} : (q - q_j) \right] \\ \text{Subjected to} : f\left(\sum, q\right) \le 0 \end{cases} \qquad \ldots(2)$$

where $\sum$ is the design variable (stress tensor) to be found, q is a vector containing the internal variables such as strain hardening and kinematic hardening variables to be found, C is the material stiffness matrix, $f(\sum, q)$ is the yield function, and E is the so-called matrix of generalized hardening moduli. One of the solutions to the above problem is the following equation for the plastic rate of deformation, [11].

$$D^P = \lambda \frac{\partial f(s,q)}{\partial s} \qquad \ldots(3)$$

In a crystal plasticity problem, the deformation is defined by several yield surfaces, and the number of yield functions depends on the number of slip systems in a crystal. Assuming the validity of the Schmid law for the plastic deformation of a single crystal, then for any slip system a yield function can be defined as:

$$fa(s,q) = \frac{|s : p^a|}{t_y^a} - 1 \qquad \ldots(4)$$

the constraints of problem (2) can be combined and replaced by an equivalent single constraint defined as:

$$f(\sigma, q) = \frac{1}{\rho} \ln\left[\sum_{i=1}^{m} \exp\left[\left(\rho \frac{|\sigma : P^{\alpha}|}{\tau_y^{\alpha}} - 1\right)\right]\right] \qquad \ldots(5)$$

where τ_y^{α} is the critical shear stress on slip plane α, and P^{α} is a matrix showing the orientation of a slip system and is defined by:

P^{α} is the symmetric part of the Schmid tensor, I^{α}, describing the orientation of a slip system, defined as:

$$P^{\alpha} = \frac{1}{2}[(I^{\alpha}) + (I^{\alpha})^T] = \frac{1}{2}(m^{\alpha} \otimes n^{\alpha} + (m^{\alpha} \otimes n^{\alpha})^T) \qquad \ldots(6)$$

where n^{α} is a unit normal to the slip plane, and m^{α} is a unit vector denoting the slip direction.

The plastic deformation matrix can be expressed as, [11]:

$$D^P = \sum_{\alpha=1}^{N} \dot{\gamma}^{\alpha} P^{\alpha} \qquad \ldots(7)$$

Where $\dot{\gamma}$ are the slip rates.

And spin tensor, which represents the material axis rotation, can be expressed as:

$$\Omega^P = \sum_{\alpha=1}^{N} \dot{\gamma}^{\alpha} w^{\alpha} \qquad \ldots(8)$$

Where w^{α} matrix is the anti-symmetric part of I^{α}, defined as:

$$w^{\alpha} = \frac{1}{2}(m^{\alpha} \otimes n^{\alpha} - (m^{\alpha} \otimes n^{\alpha})^{T}) \quad ...(9)$$

Using equation 3,5 and 7, it can be shown that during the plastic deformation of a single crystal the slip rate on any slip system could be expressed by, [12]:

$$\dot{\gamma}^{\alpha} = \lambda \frac{\frac{sgn(\sigma : P^{\alpha})}{\tau_y^{\alpha}} \exp\left[\left(\frac{\rho}{m}\frac{|\sigma : P^{\alpha}|}{\tau_y^{\alpha}} - 1\right)\right]}{m\sum_{\beta=1}^{N} \exp\left[\left(\frac{\rho}{m}\frac{|\sigma : P^{\alpha}|}{\tau_y^{\alpha}} - 1\right)\right]} \quad ...(10)$$

Where m and ρ are material parameters that control the shape of the single-crystal yield surface, and been shown to have a direct relationship with the stacking fault energy (SFE) of the material as following:

$$\rho = \frac{5\Gamma}{Gb} \times 10^{-3} \quad ...(11)$$

Where Γ is the SFE of the material, G is the shear modulus, and b is the magnitude of Burgers vector. For most materials m = 1 and parameter λ is a Lagrange multiplier which has been shown to be a measure of the rate of plastic work in a crystal,

The generalized Schmidt factor can be found for each slip system α by finding the scalar product of the normalized stress tensor (using the Frobenious norm) and the Schmidt matrix.

In order to define the resistance against the shear, Hill, [13], and Asaro and Needleman, [14], proposed the following formulation:

$$\dot{\tau}^{\alpha} = \sum_{\beta=1}^{N} h^{\alpha\beta}|\dot{\gamma}^{\beta}| \quad ...(12)$$

Where $|\dot{\gamma}^{\beta}|$ is the plastic slip rate on the active slip system β , and $h^{\alpha\beta}$ are the components of the hardening matrix $h^{\alpha\alpha}$ are known as the self-hardening moduli while $h^{\alpha\beta}$ for $\alpha \neq \beta$ are known as the latent-hardening moduli. Hutchison, [15], proposed the following model for evolution of the components of hardening matrix

$$h^{\alpha\beta} = h^{\beta}[q + (1 - q)\delta^{\alpha\beta}] \quad ...(13)$$

Here q is the so-called latent-hardening ratio, which is the hardening on a secondary slip system caused by slip on a primary slip system (Kapoorand Nemat-Nasser) [16] and can be measured by the ratio of the latent-hardening rate to the self-hardening rate of a slip system with typical values in the range of $1 < q < 1.4$. The parameter q can be considered as 1 for coplanar slip systems and 1.4 for non-coplanar slip systems. There are different kinds of hardening models presented by researchers for the evolution of h^{β} (so-called self-hardening). One of the most well-known formulations is:

$$h^{\beta} - h_0 \left|1 - \frac{\tau_y^{\beta}}{\tau_s}\right|^{a} sgn\left(1 - \frac{\tau_y^{\beta}}{\tau_s}\right) \quad ...(14)$$

where h_0, a, and τ_s are slip system hardening parameters, which are considered to be identical for all slip systems, h_0 denotes the initial hardening rate, τ_s the saturation value of the slip resistance, and a the exponent describing the shape of the stress-strain yield function. These parameters can be obtained by fitting the model to experimental data.

2.1. Calibration of CPFE Simulations

The crystal plasticity model developed by (Zamiri and Pourboghrat , [12]), for FCC metals was used to study tin. Firstly, the existing crystal plasticity model was modified in order to account for the more complicated crystal structure of tin. Tin has a body centered tetragonal crystal structure with 32 possible slip systems. Since not much is known from the literature about the slip activity of tin slip systems, slip resistance or hardening characteristics, a modified crystal plasticity model was used to simulate the deformation of solder balls under shear loading in order to identify the likely active slip systems and hardening properties that allow comparison with experiments. Due to its formulation, the crystal plasticity model calculates shear rate for each slip system, allowing the user to identify the most active slip systems for a given increment of plastic deformation. The incremental hardening of slip systems is also a function of the magnitude of shear rates, and hardening parameters. By comparing the simulation results with microscopic and macroscopic measurements, estimates for the hardening parameters of slip systems for tin were identified (Darbandi et al., [10]). Once these parameters were fitted to a set of experimental dataset, they were no longer modified when the code was used to simulate deformation of tin solder balls under different loadings

The finite element analysis was performed using commercial finite element code ABAQUS. The crystal plasticity material model was implemented using a user material subroutine in

FORTRAN (VUMAT).Solid works was used to make the model of the solder balls and ABAQUS was used to create the finite element mesh with the assignment of the boundary conditions, and building the input parameters for the analysis. The elements are 8-node linear bricks with reduced integration and hourglass control. Hourglassing can be a problem with first-order, reduced-integration elements (CPS4R, CAX4R, C3D8R, etc.) in stress/displacement analyses. Since the elements have only one integration point, it is possible for them to distort in such a way that the strains calculated at the integration points are all zero, which, in turn, leads to uncontrolled distortion of the mesh. First-order, reduced-integration elements in ABAQUS include hourglass control, but they should be used with reasonably fine meshes. Hour glassing can also be minimized by distributing point loads and boundary conditions over a number of adjacent nodes. The elastic constants for tin and copper are known and tabulated in Tables 1 and 2, respectively. The parameters used for hardening in Table 2, were chosen so that they generated trends that are commonly observed in polycrystalline or multi-joint experiments (Darveaux et al., [17]) and various single crystal experiments (Zhou , Bieler, et al., [18]).

Table 1,
Elastic Constants (GPa) of Tin used in Numerical Analysis.

Parameter	C11	C22	C33	C44	C55	C66	C12	C13	C23
	72.3	72.3	88.4	22.0	22.0	24.0	59.4	35.8	35.8

Table 2,
Hardening parameters of tin for different slip systems used in numerical analysis.

Parameter	τ_0	τ_s	h_0	a	q	m	ρ
	23 (for all sets)	40 (for all sets)	100 for sets (1,2,5,7) 150 for sets (3,4,6,8,9,10)	20 (for all sets)	1.4	1	60

3. Experimental Methods

Tin- Lead, Lead –Free solder Alloys and pure Tin (Table 3) [19], were studied, evaluating more than 500 Balls that were (420-600) microns in diameter. Each ball was individually compressed, to compare the load-displacement deformation behavior of each material. The loading stage with one ball is illustrated in Figure 1.

Table 3,
Tin, Tin-lead, and Lead-free Solder Alloys Materials.

Solder Alloys	Melting Temperature ˚C	Young's Modulus GPa	Ultimate Tensile Strength MPa
SAC305	217	54	36
Sn0.7Cu	227	43	40
63Sn37Pb	183	35	37-46
Sn3.5Ag	221	56	55
30Sn70Pb	185	32	42.30
Sn42Bi58	138	11.9	63
Sn	231.9	41-45	21.4

3.1. Ball Compression Process

The compression process was accomplished using a Rheometric Solids Analyzer instrument model RSS 111 (Figure 1) at room temperature.

Fig.1. Ball compression fixture within Rheometric Solids Analyzer machine (Compliance 6.996E-05 mm/gm.)

The compression test methodology was used to obtain the time-dependents material response of compression of a ball shaped sample. Each solder ball had a spherical diameter of (420-600) micron , this range of balls diameters was found from loading –unloading processes for each ball solder materials.

Balls were put in place on the loading platens, and centered approximately close to the loading axis. Then the instrument was calibrated to maximum cap of 600 microns (according to the maximum balls diameter range) and for each ball compression process , the instrument is setting to the reference point command cap to 600 micron , then starting compression test , loading was applied when the loading platen was lowered with simultaneous data acquisition at a rate of 0.01mm/s until a particular displacement was reached, the particular displacement was be fixed in instrument control zone by time interval of 15 sec and a rate of 0.01mm/s . Because each ball had a different diameter, the maximum strain imposed varied from sample to sample. The samples were loaded up to a given displacement of (150) microns. As each ball had a different diameter, the load reached at maximum load consequently had a displacement that varied; loading was conducted to a different displacement. 30 samples of each of 8 alloys were investigated.

3.2. Aging Processes

To investigate the effect of grain size on the loading, some alloys were aged to 150 C for 170 hours in a Carbolite Temperature Control Oven, type 3508. The microstructure of selected balls before and after aging was investigated after polishing, (but these balls were not deformed). Different samples of balls a Scanning Electron Microscope (SEM) were taken before aging processes the balls were deformed, aged.

Aging experiments were performed by placing the solder balls into CARBOLITE Temperature Control Oven, Type (3508) at aging temperature for 170 hours. Then the balls were slightly polished to remove the oxide layer resulting from to reveal the change in microstructure. Scanning electron micrographs of different balls were taken before and after aging process to compare grain growth.

4. Results and Discussion

4.1. Compression Test Results

During the compression processes various deformation behaviors occurred which represent the variation in mechanical property variability for different alloys. This clear in loading–unloading processes and in Maximum–Loading processes.

Figure (2) a shows the loading –unloading curves of SAC305 alloy chosen from a batch of solder balls supplied by a manufacturer, during compression and unloading process. The load displacements data were shifted along the displacement axis until one of the datum points close to 50 gm was reset to 0 displacement so that all of the curves would have a nearly common initial loading point, to assist comparison. Figure (2) b shows the same data without unloading data so that the difference in loading behavior can be more clearly observed. From the known initial and final displacement values, different original ball diameter between (426- 449) microns were identified. From Figure (2) b different deformation behaviors each ball are apparent, particularly with regard to the loading slopes of each ball. Balls 15 and 19 show representative value of relatively hard, soft, and in-between deformation behavior. From the load magnitude for these two balls at the same displacement, different load values vary by a factor of 25%.

The deformation of Sn0.7Cu alloy shows in Figure (3) a loading –unloading and max.-load deformation in Figure (3) b. The loading-unloading deformation behavior shows different slope (different Young Modulus), balls 16, 14, and 15 show very clear that differences. Different maximum load deformation behavior and magnitudes can be shown in Figure (3) b, for balls 17, 3, and 13 have different amount of deformation with same amount of load.

For 63Sn37Pb Figure (4) a shows the different deformation behavior for loading –unloading slopes and that is clear in different behavior of two groups of balls. Figure (4) b shows different maximum load against same deformation magnitude especially for balls 2, 9, 6, and 5.

Sn3.5Ag alloy balls show also different loading-unloading deformation behavior for different balls diameter Figure (5) a shows a different unloading slope and that clear for samples 14,2,12, and 1. Figure (5) b shows the maximum loading deformation of Sn3.5Ag balls, as we see for displacement of 0.03 mm (ball 13) needs about 110 gm force ,while for (ball 9) which has less deformation amount of 0.022 mm needs more than 130 gm force for maximum deformation.

Figures (6) a and b show loading –unloading and maximum load deformation processes for 30Sn70Pb alloy respectively , variety in unloading slope for some balls like Balls 5, 7, 1, and 9 than others. Maximum load deformation processes shows large difference deformation interval nearly for same force comparing with others by a factor of 50%.

Sn42Bi58 loading-unloading Processes in Figure (7) a, the load displacements data were shifted along the displacement axis until all the datum points close to 50 gm so that all of the curves would have a nearly common initial loading point, to assist comparison. All balls have same unloading slope and same deformation behavior .Max. Load deformation in Figure (7) b, shows the difference appears in high deformation after 0.260 gm. loading force, some balls need about 300 gm. for 0.070 mm deformation interval but we find that other balls need about 380 gm. for same deformation interval.

Sn loading –unloading deformation processes shown in Figure (8) a, unloading slope shows that for all balls have same plastic deformation behavior, the difference in interval magnitude comes from the difference in manufacturing balls diameters as received. Figure (8) b, shows different maximum load magnitude for same deformation interval can see that clear for balls 16, 6, 11, 14, and 5 for same amount of 0.095 mm distortion need different amount of force from 106.5 gm. to 260 gm.

4.2. Aging Processes Results

Figures (9-22) show SEM Images for microstructure of different alloy Samples at room temperature and after aging processes at 150˚C for 170 hours. The optical and polarized images of SAC305microstructure in Figure 9 (a) shows alight region Sn-rich phase, Ag_3Sn participate particles, and small dark particles of Cu, while in (b) reveals a crossed polarize picture of as received ball. Optical and polarized images in Figure (10) a and b after aging process, a shows significantly ball microstructural changes and its stability under isothermal aging condition and coarsening of Sn particles. In b the polarized image shows three large regions with different colors (corresponding to no more than three main Sn grain orientations).

Figure (11) a and b shows the Sn0.7Cu microstructure before aging, greater tin concentration with light appearance and small black particles of Cu. Figure (12) a and b shows the grain enlargement of Sn grains which appear clear in b.

Optical micrographic and polarize image for 63Sn37Pb Sample before aging are shown in Figure (13), bright color of Sn-rich grains and grey Pb shown by arrows in a, while in b the crossed polarizer picture shows at least two different colors represent the Sn grains orientation . Figure (14a) shows the change its microstructure after aging process represent by Sn grain enlargement and orientation that is shows more clearly in b of different colors of Sn grains.

Figure (15) a and b shows the optical and polrized micrograph for Sn3.5Ag alloy solder before aging , in a shows the Sn grain of light color, while Ag3Sn participate particles with gray color.In b the polorized image shows the different colors represantive by Sn-rich orentation grains. The microstructure changes shown singfictaly in Figure (16) a and b after aging process, and at least tow different colors of Sn grains can be seen in b.

The distribution of Sn and Pb grains structure of tin-lead alloy 30Sn70Pb before aging is shown in Figure (17) a and b, Sn grains with light color and Pb-rish with dark color. The microstructure of solder after aging process shown in Figure (18) a and b with no scientifically Sn grains orientation.

Figure (19) shows the microstructure images for Sn42Bi58 alloy before aging process in a as optical and in b as polarized with homogenous distribution of Sn and Bi grains. After aging process, the microstructure was changed, as we see in Figure (20) a and b, Sn grains enlargement and orientation was revealed by a crossed polarizer picture in b.

Pure Sn as received before aging is shown in Figure (21) a and b, the irregular cross section ball as a result of polishing work and the softened of pure Sn Ball, in b, t two different colors appear according to the Sn grain orientation. Figure (22) a and b show the homogenous and enlargement Sn grains structure after aging process.

4.3. Simulation Results

Simulation approach was done on two of solder materials SAC305 as a Lead-Free solder alloy and the second 30Sn70Pb as a Tin-lead based solder alloy to compare the deformation behavior for each solder. The simulation approach results are represented by two Figures (23) and (24).

According to the compression deformation results, the different behavior of each material during compression deformation and its effect on variable the properties of solder balls, which interpret the anisotropy grain behavior for SAC305, as shown in Figures (2) a and b . Anisotropy is very strong in Sn and has large effect on the reliability , the fracture probability in lead –based solder alloy is different from that in Lead-Free solder alloys, mostly because of the anisotropy present in Tin phase [20]. That is clear in variety in Loading –Unloading slope and also in the different amount of Maximum load for some ball during deformation .This behavior is clear in the microstructure of SAC305 before and after aging. The orientation of grain illustrate very clear the anisotropy behavior of Sn grain Figures. (9) and (10) and also is illustrated in Simulation Figure (23).

When material is formed, the grains are usually distorted and elongated in one or more direction which makes the Martials Anisotropy. As the microstructure of solder coarsening during the aging process, it is necessary to investigate its influence on the mechanical properties of the solders.

The characterization of lead –Free solder, especially after isothermal aging, is very important in order to accurately predict the reliability of solder balls, and the grain size and morphology have significant effect on the mechanical properties of sub-mm scale balls.

Optical micrographs show bright field image of as an received sample , while polarized micrographs reveal a crossed polarizer picture of solder ball, it can be seen that large region with different colors corresponding to main Sn grain orientation increase in aging samples.

The Simulation approach supported the experiments results for SAC305 and that is shown in Figure (23), the isotropic model is too far from the experimental results showing that isotropic hardening overestimates the hardening .The anisotropy of Sn grains in SAC305 lead-free solder alloy interpret the different behavior of deformation of balls and its effect on mechanical proprieties like Modulus of elasticity, Strength, and Reliability. Simulation results of compression tests for 30Sn70Pb in Figure (24) are showing that the isotropic model matches well with experimental data.

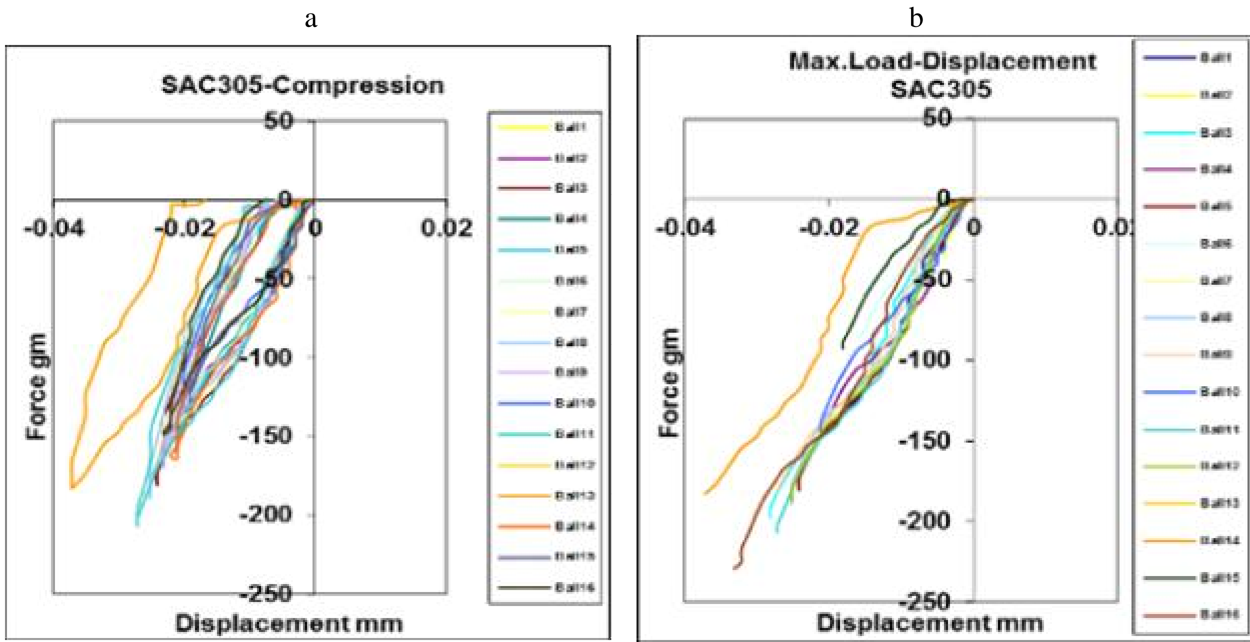

Fig. 2. (a) SAC305 Loading-Unloading and (b) SAC305 Loading to maximum load.

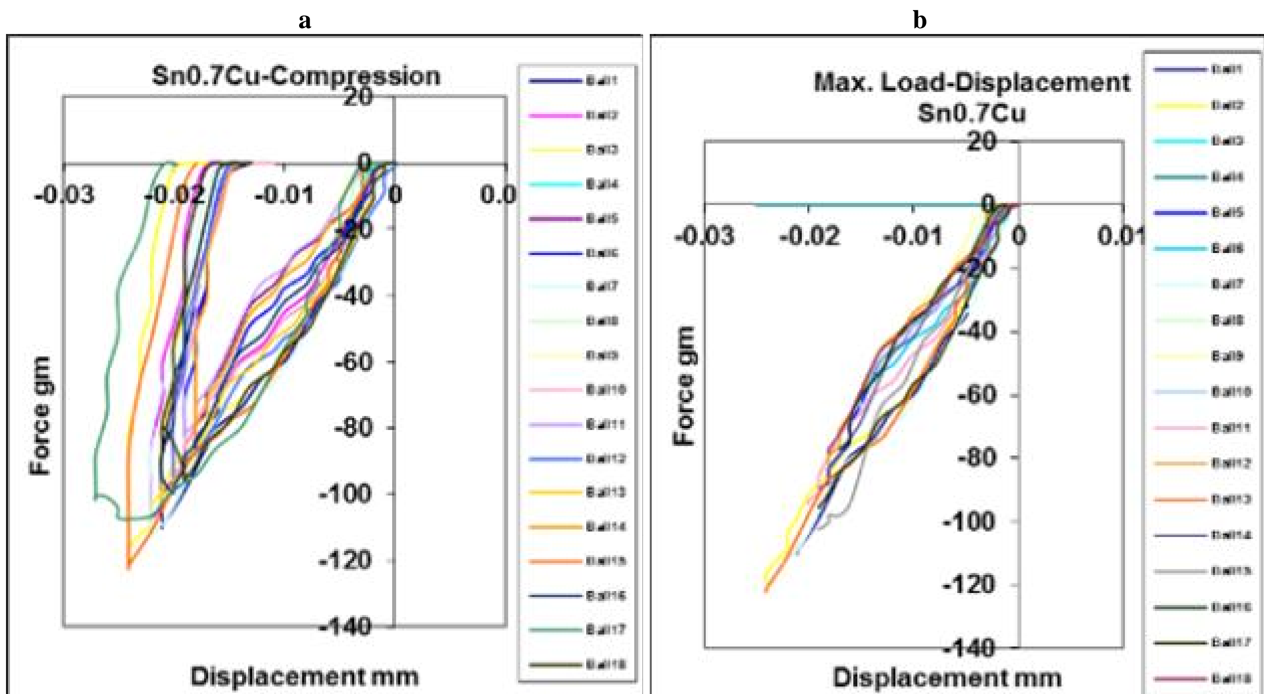

Fig. 3. (a) Sn0.7Cu Loading-Unloading and (b) Sn0.7Cu Loading to maximum load.

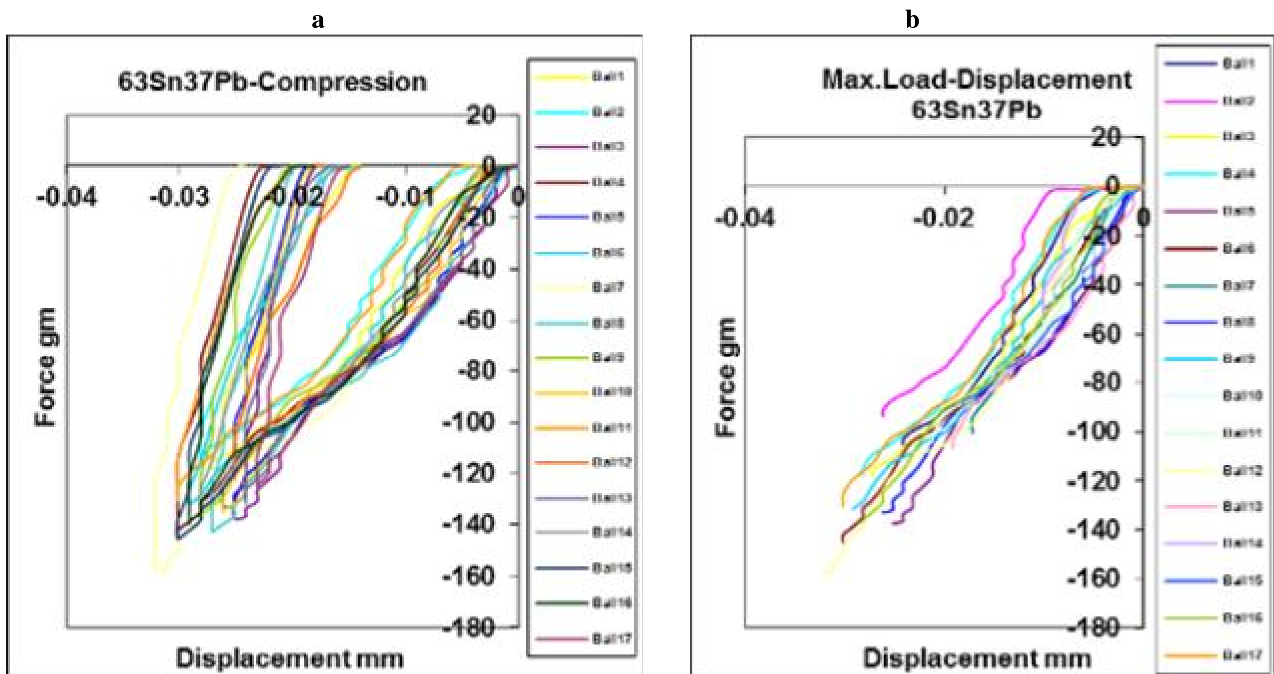

Fig. 4. (a) 63Sn37Pb loading-unloading and (b) 63Sn37Pb loading to maximum load.

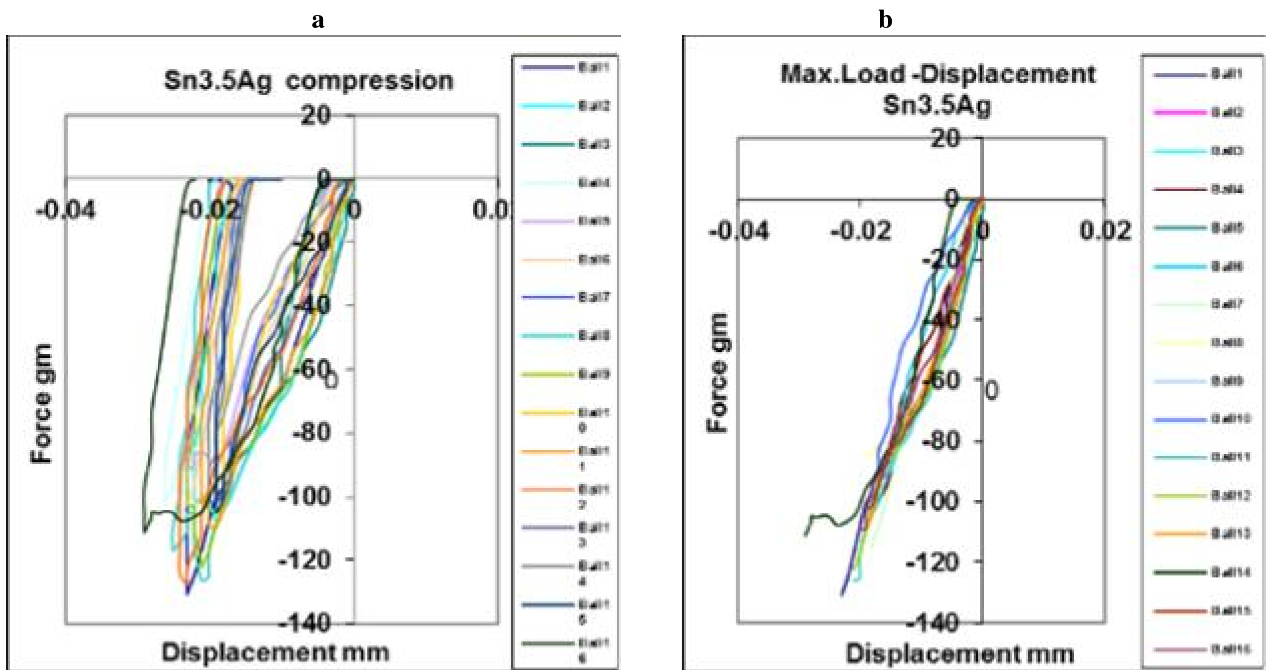

Fig. 5. (a) Sn3.5Ag Loading-Unloading and (b) Sn3.5Ag Loading to maximum load.

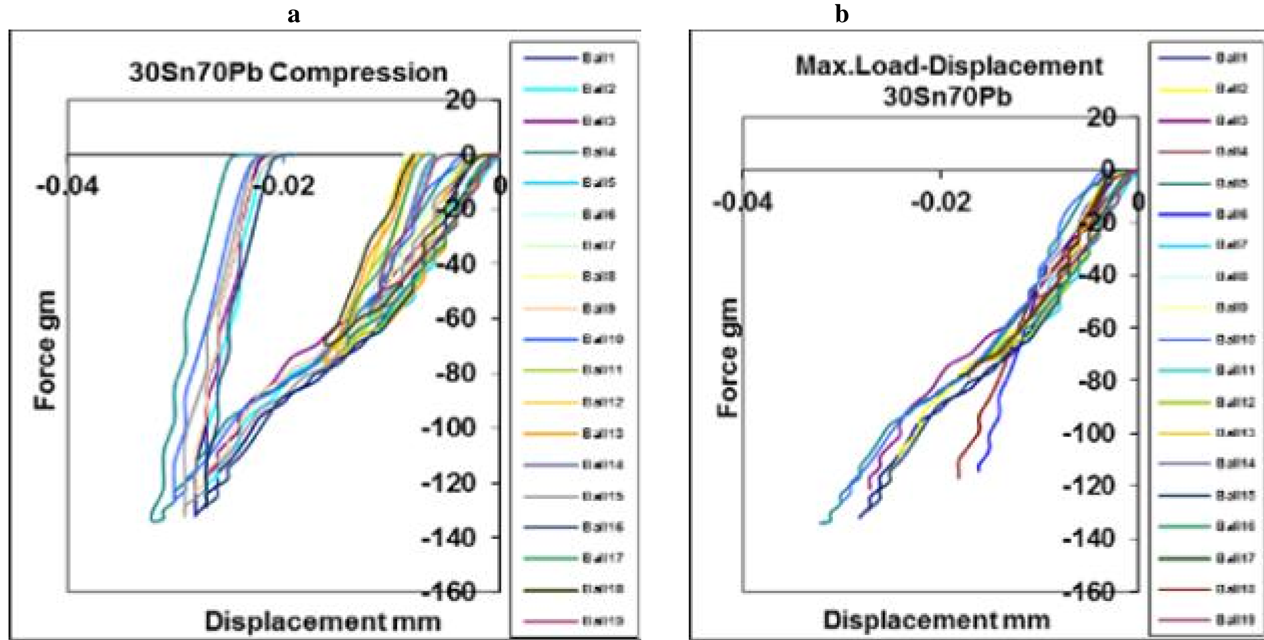

Fig. 6. (a) 30Sn70Pb Loading-Unloading and (b) 30Sn70Pb loading to maximum .

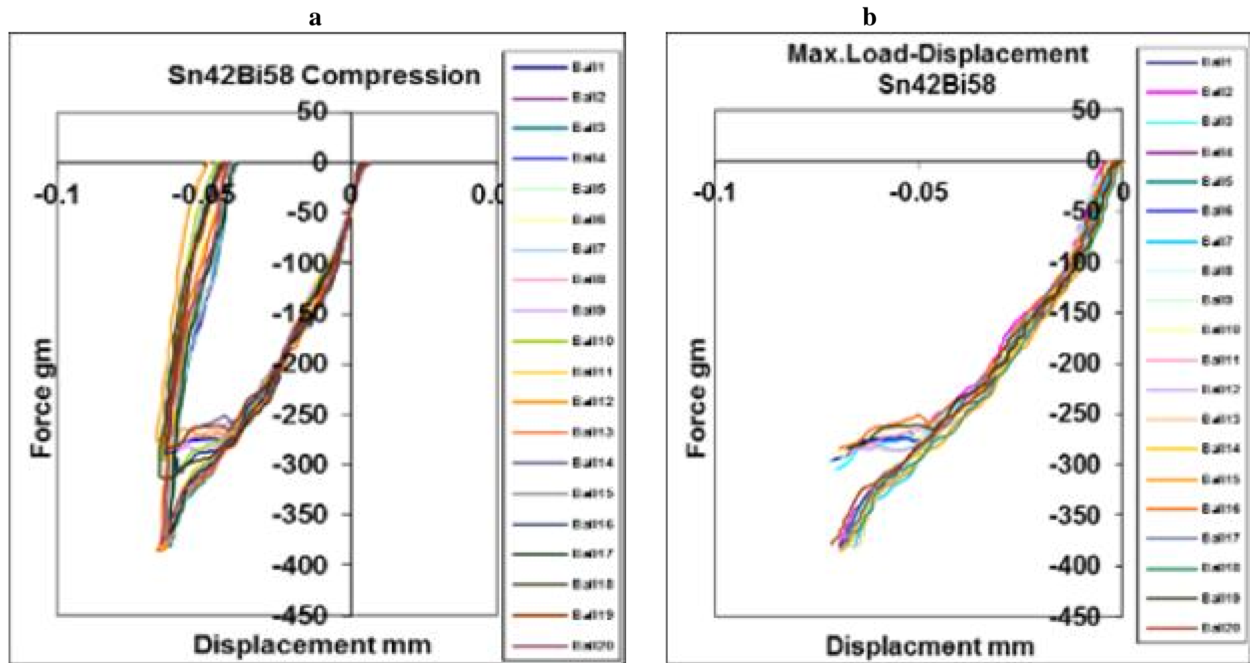

Fig. 7. (a) Sn42Bi58 Loading-Unloading and (b) Sn42Bi58 Loading to maximum load.

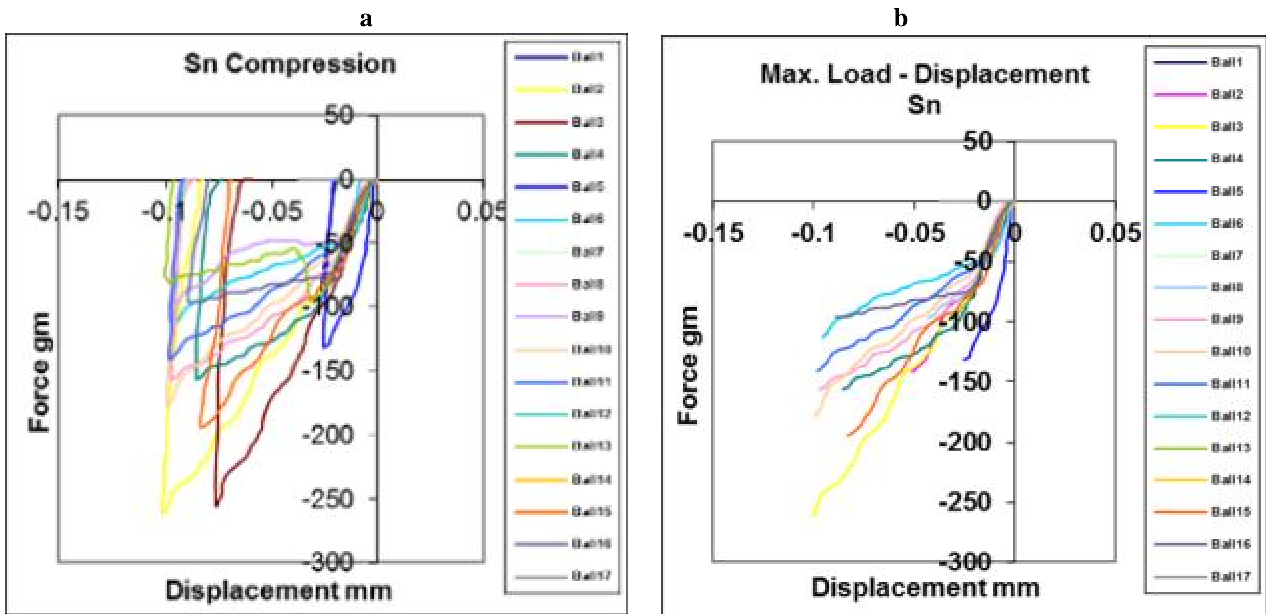

Fig. 8. (a) Sn Loading-Unloading and (b) Sn Loading to maximum load .

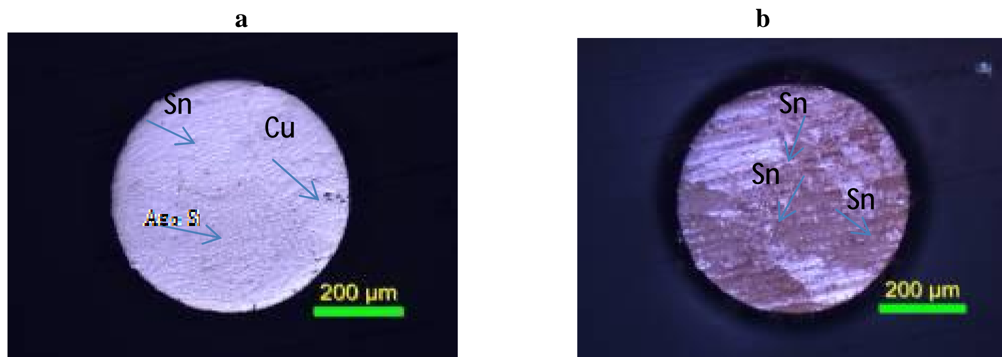

Fig. 9. SAC305 microstructure Images before aging(a-Optical image and b-Polarize image).

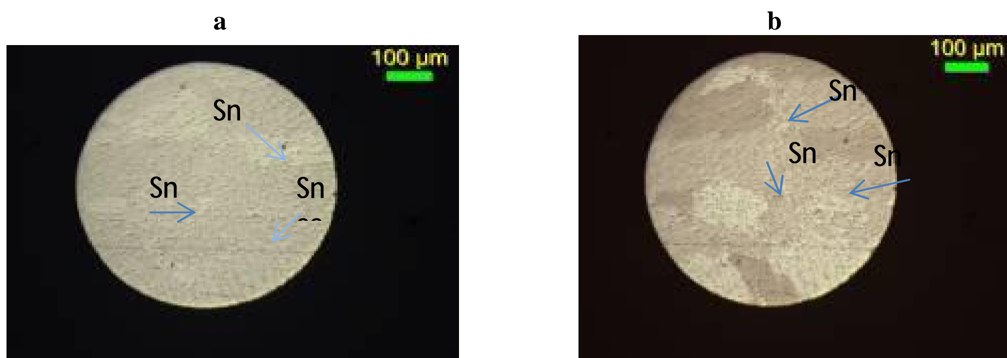

Fig. 10. SAC305 microstructure Images after aging (a- Optical image and b-Polarize image).

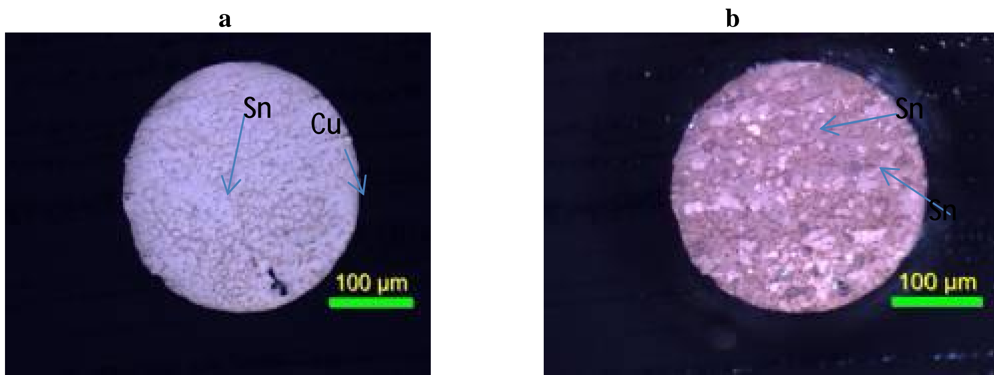

Fig. 11. Sn0.7Cu microstructure Images before aging (a- Optical image and b-Polarize image).

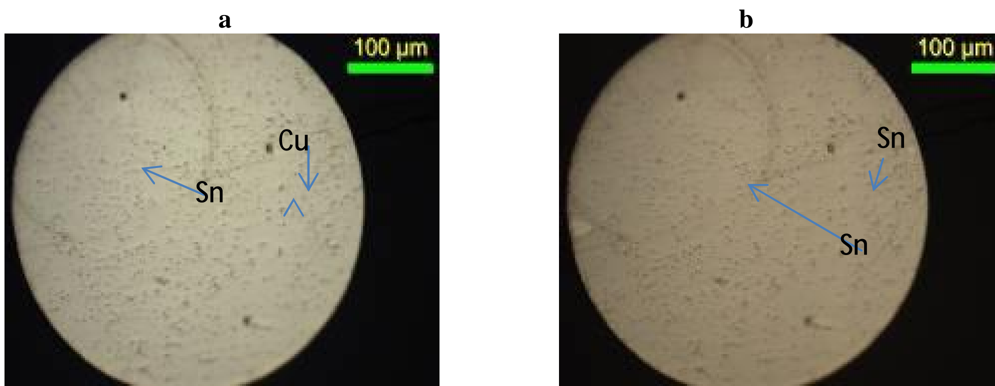

Fig. 12. Sn0.7Cu microstructure Images after aging (a- Optical image and b-Polarize image).

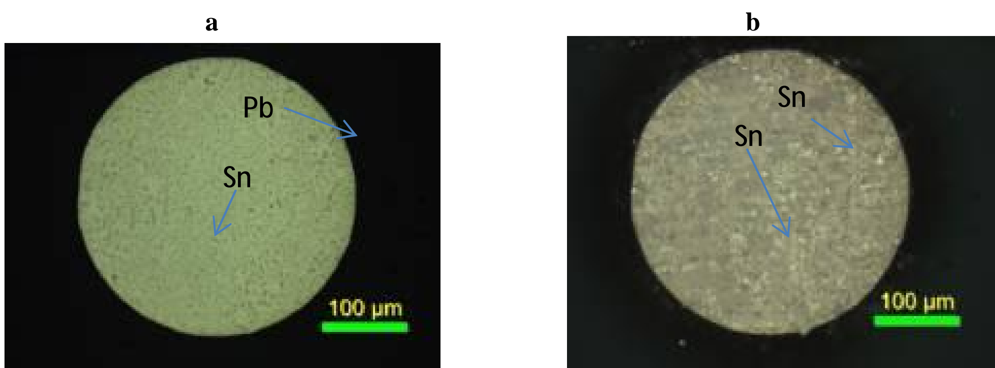

Fig. 13. 63Sn37Pb microstructure Images before aging(a-Optical image and b-Polarize image).

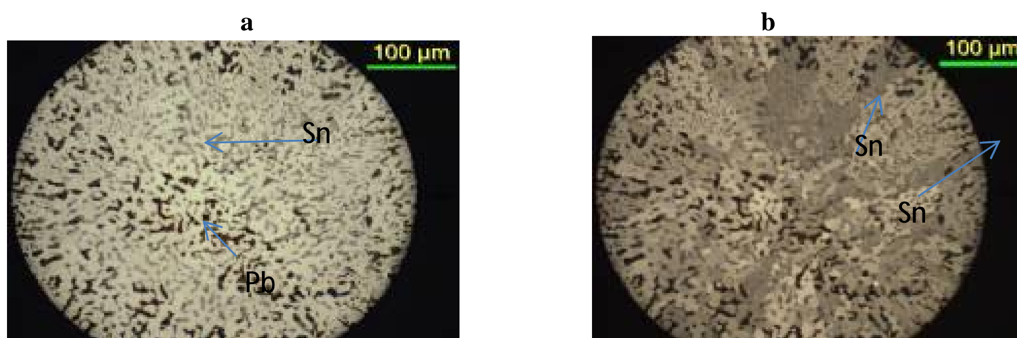

Fig. 14. 63Sn37Pb microstructure Images after agin (a-Optical image and b-Polarize image).

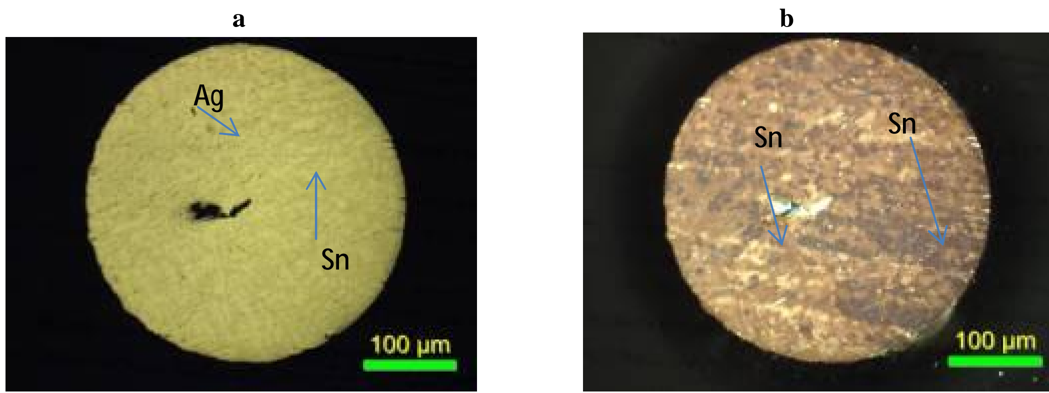

Fig. 15. Sn3.5Ag microstructure Images before aging (a- Optical image and b-Polarize image).

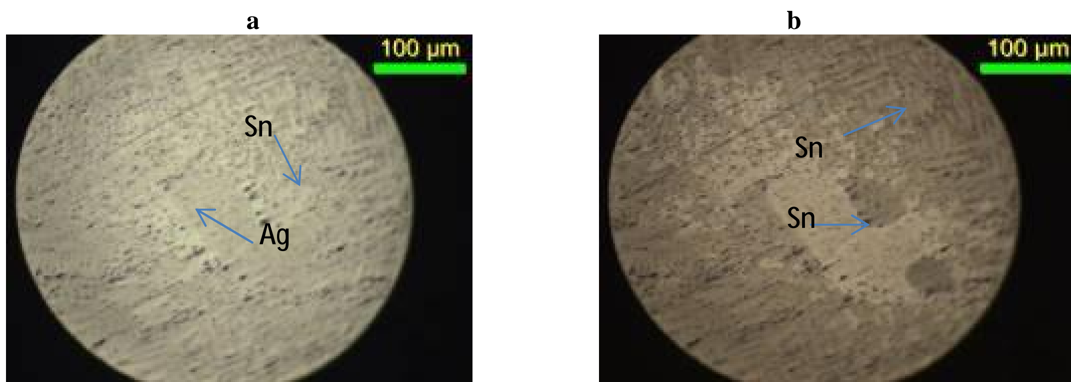

Fig. 16. Sn3.5Ag microstructure Images after aging (a- Optical image and b-Polarize image).

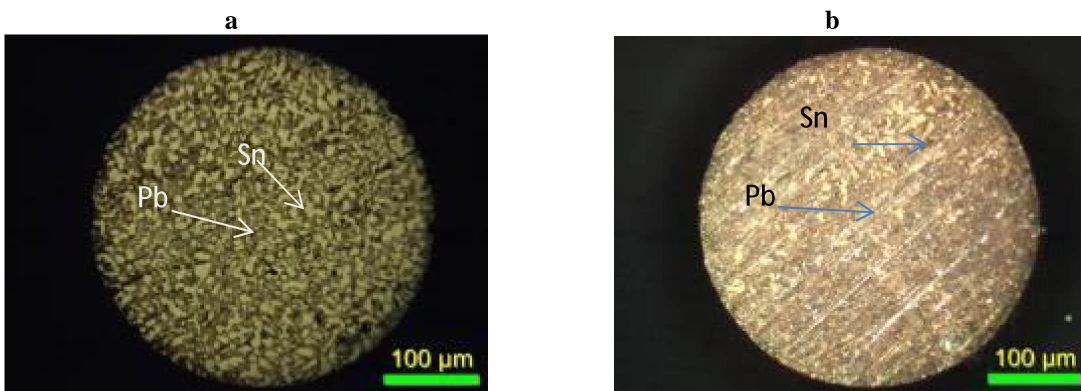

Fig. 17. 30Sn70Pb microstructure Images before aging (a- Optical and b-Polarize image)

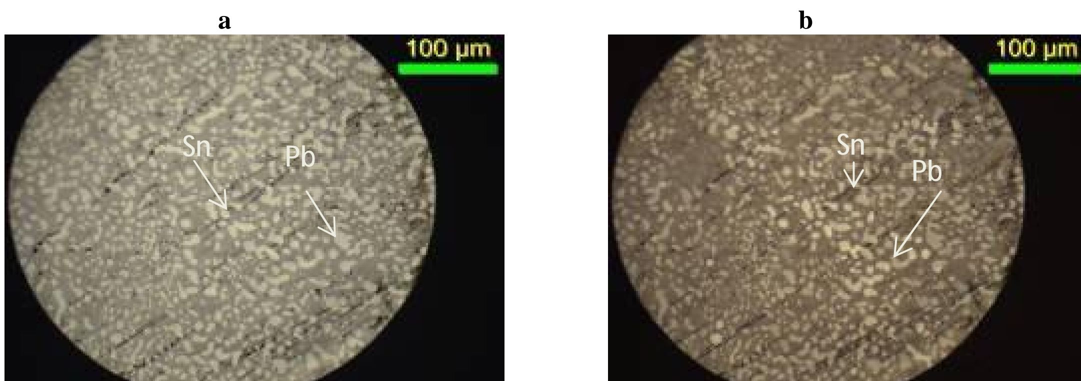

Fig. 18. 30Sn70Pb microstructure Images after aging (a-Optical image and b-Polarize image).

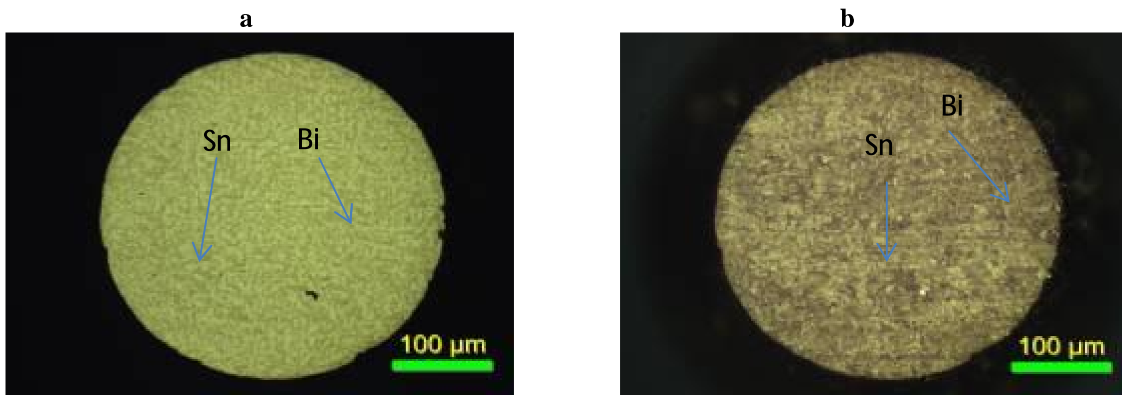

Fig. 19. Sn42Bi58 microstructure Images before aging (a-Optical image and b-Polarize image).

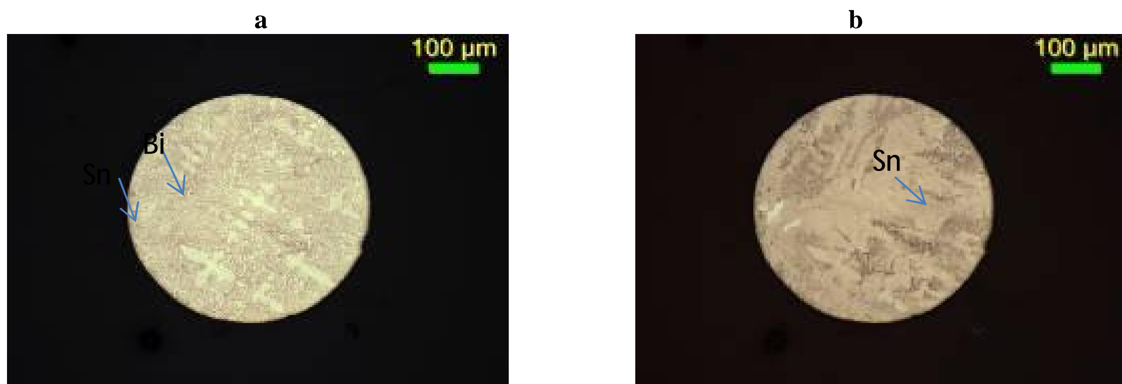

Fig. 20. Sn42Bi58 microstructure Images after aging (a-Optical image and b-Polarize image).

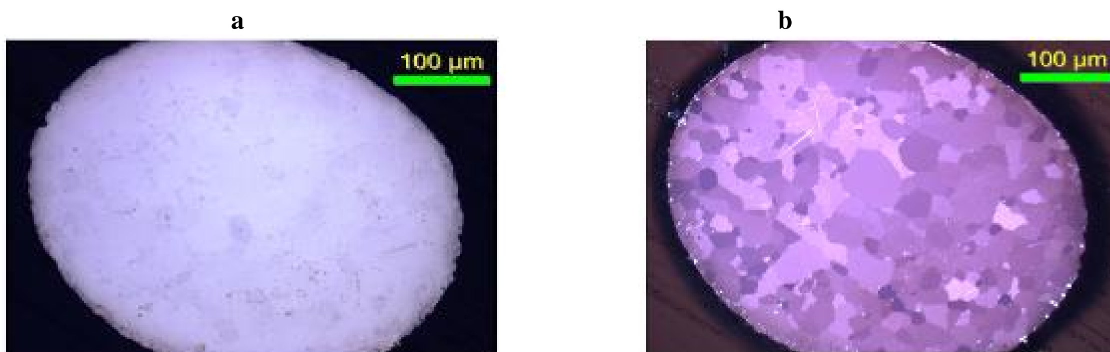

Fig. 21. Sn microstructure Images before aging(a-Optical image and b- Polarize image).

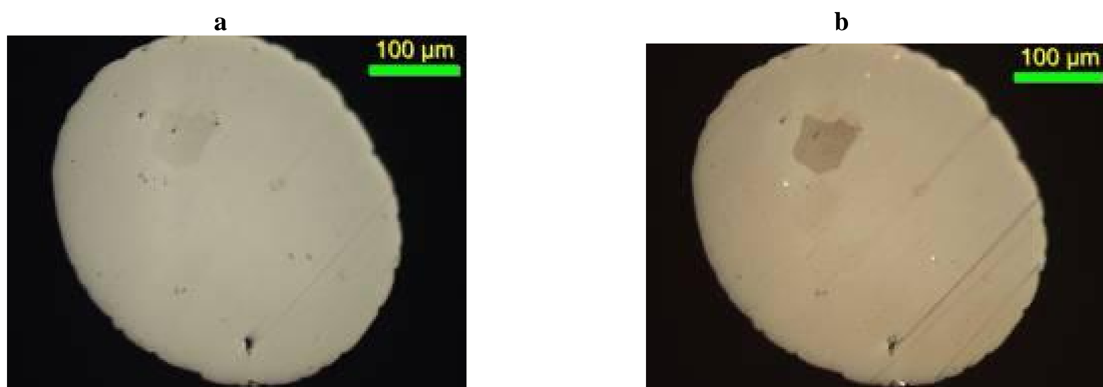

Fig. 22. Sn microstructure Images after aging (a- Optical image and b- Polarize image).

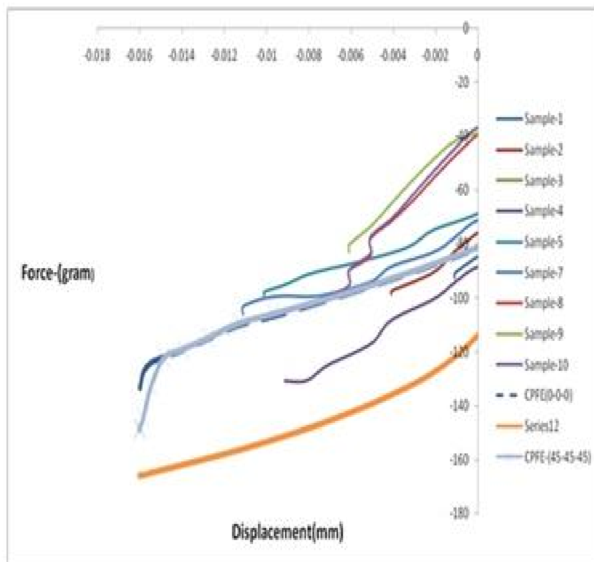

Fig. 23. SAC305 Compression Simulation .

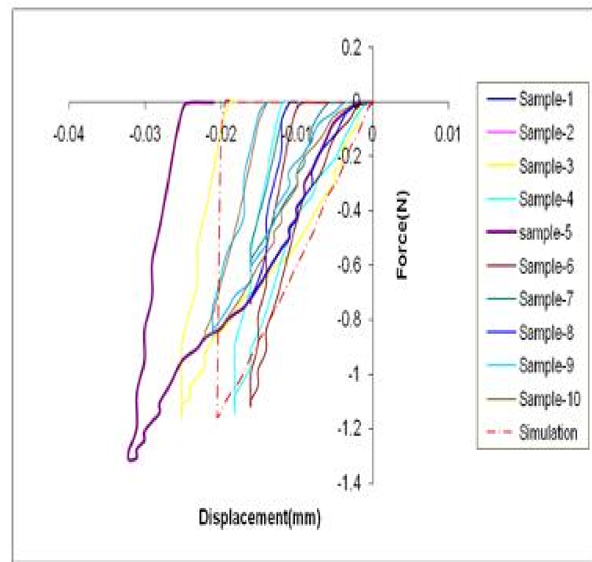

Fig. 24. 30Sn70Pb Compression Simulation.

5. Conclusions

Compression deformation of different metals of tin-lead and lead-free solders and aging processes at 150 ˚C for 170 hours were done in order to get a comprehensive understanding the mechanical properties of the solders during deformation behavior and isothermal aging processes, and from the experimental and simulation results we can conclude the following:

1. Loading-Unloading deformation processes give good understanding the variety if deformation behavior and its effect on mechanical properties and the relation of Maximum Load –Displacement show clearly interrelation between the magnitude of elastic-plastic deformation with Anisotropy phenomena of tin-rich lead-free solder alloys.
2. Aging processes at 150 ˚C for 170 hours is suitable for alloy aged –softened and this softening correlated with the growth of relatively large tin- rich crystals and the coercing of Sn particles.
3. CPFE model can solve the mechanical deformation behavior of materials under compression effect. For SAC305 as a lead-free solder the Simulation results for compression test showing that since the plastic deformation occurs in a small region of the sample, the difference between differed orientations is observed in large deformation. As is highlighted, the isotropic model is too far from the experimental results showing that isotropic hardening overestimated the hardening.
4. Simulation result for tin-lead solder 30Sn70Pb c compression matches the experimental data are interpreting the homogenous deformation behavior of 30Sn70Pb balls as a Tin-lead solder and support its isotopic phenomenon.
5. The different specification of manufacturing balls as received like sizes and different deformation behavior give us scientifically effect on the mechanical properties which must be taken into consideration by manufacturer and suppliers.
6. The fact that the microstructure remains stable under isothermal aging conditions is beneficial for manufacturing operation when reflow of solder joints.
7. Further investigation and study that can be done by reflow same materials and testing as solder joints and compare with present results.

Acknowledgment

The Author presents thanks to Institute International Education & SRF for their cooperation and supporting. Greatly appreciate and thank to Professor Andre Lee for his supports and cooperation and also to Professor Tom Bieler for his advices and reviewing. The author also thanks Professor Farhang Pourboghrat for his kind cooperation. Many thanks to Dr. Payam Darbandi for his kind help in simulation process. Also many thanks to Quan Zhou and Yang Lu for their assistance in aged samples preparation and testing.

6. References

[1] Andree Lee, Deep Chouduin, and K.N Subramiuman , Lead-free Solders: Materials
a. Reliability for Electronics, First Edition. Edited by K. N. Subramanian, (2012), p. 273.

[2] R.A. Lebenson and C.N. Tome, “A self-consistent Anisotropy Approach for the
a. simulation of Plastic Deformation and texture development of Polycrystals Application
b. to Zirconium Alloys, Acta Metal. Mater. 41, 2611 (1993).

[3] A.U.Telang and T.R.Bieler, “The orientation imaging microscopy of Lead-free Sn-Ag
a. solder joints”, JOM. June (2005), pp. 44-49.

[4] H.F.Zou , Z.F.Zhany, “ Effect of aging time , strain rate and solder thickness on
a. interfacial fracture behaviors of Sn-3Cu/Cu Single Crystal joints” , Microelectronic
b. Engineering 87 (2010) 601-609

[5] Karl Seeling and David Suroski, AIM, Incorporated.

[6] P.Kumar, Z.Huang, I. Dutta, G. Subbarayan, and R. Mahajan, Lead-free Solders:
a. Materials Reliability for Electronics, First Edition. Edited by K. N. Subramanian,
b. (2012), p. 197.

[7] Q.K.Zhany, O.S.Zhu, Z.F. Zhang, “Fracture mechanism and strength-influencing
a. factors of Cu/Sn-4Ag Solder joints aged for different times, Materials Science and
b. Engineering A 527 (2010) 1367-1376.

[8] Qiang Xiao, Luu Nguyen, William D.Armistrong, “Aging and Creep Behavior of
a. Sn3.9Ag0.6Cu Solder Alloy”, Electronic Components and Technology Conference,
b. (2004), pp.1325 -1332.

[9] Thomas R. Bieler, Bite Zhou, Lauren Blair, Amir Zamir, Payam Darbandi, Farhang
a. Pourboghrat, Tae-Kyu Lee, and Kuo-Chuan Liu, “The Role of Elastic and Plastic
b. Anisotropy of Sn in Recrystallization and Damage Evolution during Thermal Cycling in
c. SAC305 solder Joints”, J. of Electronic Materials, Vol. 41, No. 2, 2012, pp. 283-301.

[10] P.Darbandi, T.R. Bieler, F. Pourboghrat, and Tae-Kyu Lee, “Crystal Plasticity Finite-
a.Element Analysis of Deformation Behavior in Multiple Grained Lead-Free Solder
b. Joints”, Journal of Electronic Materials, Vol. 42, Issue 2, (2013), pp. 201-214

[11] A.Zamiri, T.R. Bieler, and F.Pouboghrat, “Anisotropic Crystal Plasticity Finite Element
a.Modeling of Effect of Crystal Orientation and Solder joint Geometry on Deformation after Temperature change, J. Electron Mater. 38, 231 (2009).”

[12] A.R.Zamiri and F.Pouboghrat,” A novel yield function for single crystal based on combined constraints optimization, Int.J. Plast 26, 731 (2010).

[13] R.Hill, “Generalized constitutive relations for incremental deformation of metal crystals by multislip”, J.Mech. Phys.Solids 14, 95 (1966).

[14] R.J. Asaro and A. Needleman,” Overview no. 42 Texture development and srain hardening in rate dependent polycrystals”, Acta Metall. 33, 923 (1985).

[15] J.W. Hutchison,” Bounds and self-consistent cistimates for creep of polycrystalline materials, Proc.R. Soclond. Ser. A139, 247(1976).

[16] R. Kappor and S. Nemat-Nasser, ” High-rate deformation of single crystal tantalum Temperature dependence and latent hardening, Scripta Mater. 40, 159 (1999).

[17] R. Darveaux et al., “Solder joint fatigue life of fine Pitch BGAs-impact of Design Microprocessors, Electronic Components and Technology Conference (2005

[18] B. Zhou, T.R. Bieler, T.-K. Lee, and K.-C. Liu,” Methodology for Analyzing Slip Behavior in Ball Grid Array Lead-Free Solder Joints after Simple Shear, J. Electron. Mater. 38, 2702(2009)

[19] Dr.Thomas Siewert, Dr. Stephen Liu, Dr. david R. Smith, Mr. Juan Carlos Madeni, “Database for Solder Properties with Emphasis on New Lead-Free Solders”. National Institute of Standard and Technology &Colorado School of Mines, February (2002).

[20] [20] J.Gong, C.Liu, P.P.Conway, and V.V.Silberschmidt,” Mesomechanical modeling of SnAgCu solder joints in flip chip”, Compute. Mater. Sci. 39, 187(2007).

مقارنة الخواص الميكانيكة لمواد اللحام الحاوية على الرصاص والخالية منه والمستخدمة في تصنيع الكارتات الألكترونية

علاء حسن علي
قسم هندسة المواد / الجامعة التكنولوجية
تفرغ علمي في قسم الهندسة الكيمياوية وعلم المواد / جامعة ولاية ميشيكان الأمريكية
البريد الألكتروني:dr_alaahassan@yahoo.com

الخلاصة

تركزت هذه الدراسة على التحقق من خواص الانضغاط الميكانيكية للسبائك الكروية للقصدير المحتوي على الرصاص والخالي منه باستخدام اكثر من ٥٠٠ عينة لتحديد التباين الاحصائي في خواص كل سبيكة ، كما تم استخدام التعتيق الحراري لدراسة ومقارنة تاثيره على الخواص والبنية المجهرية.
اظهرت النتائج بشكل واضح ظاهرة تباين الخواص اللدنه والمرنه لطور القصدير في السبائك الخالية من الرصاص ومقارنة النتائج العملية مع عملية التمثيل باستخدام طريقة العناصر المحددة والتي اظهرت نتائج متقاربة مع النتائج العملية و اشارت الى القيم المتوقعة من الخواص المتباينة للقصدير.